Journal of Power Sources 242 (2013) 99–105

Contents lists available at SciVerse ScienceDirect

Journal of Power Sources

journal homepage: www.elsevier.com/locate/jpowsour

Dynamic response performance of proton exchange membrane fuel cell stack with Pt/C–$RuO_2 \cdot xH_2O$ electrode

Lu Lu, Hongfeng Xu*, Hong Zhao, Xin Sun, Yiming Dong, Ruiming Ren

Liaoning Provincial Key Laboratory of New Energy Battery, Dalian Jiaotong University, Huanghe Road 794#, Dalian 116028, People's Republic of China

HIGHLIGHTS

- The average particle size of $RuO_2 \cdot xH_2O$ is 8 nm.
- A 10-cell stack is assembled using MEA with and without $RuO_2 \cdot xH_2O$.
- The performance of the MEA with $RuO_2 \cdot xH_2O$ is slightly better.
- The dynamic response performance is slightly better when $RuO_2 \cdot xH_2O$ is added.

ARTICLE INFO

Article history:
Received 15 February 2013
Received in revised form
12 May 2013
Accepted 14 May 2013
Available online 28 May 2013

Keywords:
Proton exchange membrane fuel cell
Dynamic response
$RuO_2 \cdot xH_2O$
Voltage undershoot

ABSTRACT

The dynamic response performance of a proton exchange membrane fuel cell (PEMFC) significantly affects its durability and reliability. Thus, the improvement of the dynamic performance of PEMFC has become the key for prolonging the PEMFC life in fuel cell vehicle applications. In this study, $RuO_2 \cdot xH_2O$ is prepared by sol–gel method, and then sprayed onto catalyst layers to promote PEMFC dynamic response performance. The prepared $RuO_2 \cdot xH_2O$ is characterized by TEM, which shows that the average particle size of $RuO_2 \cdot xH_2O$ is 8 nm and that the particulates are uniformly distributed. A 10-cell stack is assembled using membrane electrode assembly (MEA) with and without $RuO_2 \cdot xH_2O$. This stack is studied under various loading cycles and operating conditions, including different air stoichiometries, relative humidities, and loading degrees. Results show that the steady-state performance of the MEA with $RuO_2 \cdot xH_2O$ is better than that in the MEA without $RuO_2 \cdot xH_2O$ with a decreasing relative humidity from 80% to 20%. A slower and more unstable dynamic response of the MEA without $RuO_2 \cdot xH_2O$ is observed as air stoichiometry and relative humidity decrease as well as the loading increase. Thus, $RuO_2 \cdot xH_2O$ improves the dynamic response performance, indicating that $RuO_2 \cdot xH_2O$ can buffer the voltage undershoot, improve the stability, and prolong the lifetime of the PEMFC stack.

1. Introduction

Proton exchange membrane fuel cell (PEMFC) is used in various applications, such as portable power, transportation, and distributed power generation [1]. PEMFCs provide advantages for several applications, such as efficiency improvement, reliability, operational characteristics, zero emission, and high-energy density [2]. Among these PEMFC applications, the power system of mobile vehicles is one of the most important technologies that have been developed by PEMFC researchers [3,4]. In such a mobile power system, the transient behavior and the corresponding characteristic times have important functions in determining the PEMFC dynamic performance. For example, the time interval from the start of the operation to the steady state of the PEMFC is one of the most important characteristic times and depends largely on the dynamic response time constants of each PEMFC component.

However, the energy output process of PEMFC involves electrochemical reaction, gas transfer, proton transfer, and electron transmission. These processes occur one after another. Instantaneous current causes the PEMFC output voltage to decrease to 0 or even reach a negative value, thereby affecting the PEMFC lifetime. Thus, the development of power assistance for PEMFCs is necessary. Dynamic PEMFC responses should also be investigated to change the external load and operating parameters, improve the dynamic response performance, and lessen the damage to PEMFCs. During dynamic operations, such as start-up and acceleration, oxidant starvation may occur because of the gas response rate that lags the loading rate. This phenomenon induces the voltage

* Corresponding author. Tel./fax: +86 411 84106713.
E-mail address: hfxu@fuelcell.com.cn (H. Xu).

0378-7753/$ – see front matter © 2013 Elsevier B.V. All rights reserved.
http://dx.doi.org/10.1016/j.jpowsour.2013.05.058

undershoot or even cell reversal and further affects the durability and reliability of fuel cells [5,6]. Hence, the dynamic characteristics of PEMFCs should be improved to prolong the PEMFC life in fuel cell vehicle applications. However, most of the studies on PEMFC have focused on a stable operation; only a few authors considered the transient behaviors of stacks. For instance, Yan et al. [7] studied the transient characteristic of the PEMFC stack during dynamic loading, in which the local current and temperature increase when loaded rapidly. The extent of temperature fluctuation during dynamic loading is significantly influenced by air stoichiometries, loading rates, and air relative humidities. Yan et al. [8] further investigated the dynamic PEMFC behaviors under a series of feed gas flowrates, temperatures, pressure decreases, and relative humidities. The results of their experiments indicated that overshoot and undershoot behavior occur upon loading off and on, respectively.

Ultracapacitors are energy storage devices similar to batteries but have long life cycles compared with batteries. The fast charging and discharging abilities of ultracapacitors can be effectively utilized for dynamic load-based applications. Hydrous ruthenium oxide ($RuO_2 \cdot xH_2O$) is a mixed (electron and proton) conductor that can be used as a potential material for PEMFC [9]. $RuO_2 \cdot xH_2O$ is also the material used in pseudocapacitors because it has high stability, high specific capacitance, and rapid Faradaic reaction [10–12]. However, $RuO_2 \cdot xH_2O$ requires carbon with a high surface area to improve its utilization. The proton conductivity of ruthenium oxide is caused by solid-state surface redox transitions of ruthenium species and can be schematically written as follows:

$$RuO_x + \delta H^+ + \delta e^- \leftrightarrow RuO_{\chi-\delta}(OH)_\delta \quad 0 \le \delta \le \chi$$

The transitions proceed reversibly across the potential region in fuel cell operations [13].

Some studies have demonstrated the suitability of $RuO_2 \cdot xH_2O$ as an anode catalyst support for PEMFC [14,15]. For instance, Sun et al. [16] prepared $RuO_2 \cdot xH_2O$ by using the sol–gel method and adhered $RuO_2 \cdot xH_2O$ on a Nafion membrane surface based on the Czochralski method. Wu et al. [17] also prepared $RuO_2 \cdot xH_2O$/CNTs by the sol–gel method and sprayed $RuO_2 \cdot xH_2O$/CNTs onto the Pt/C electrode surface to form the cathode. $RuO_2 \cdot xH_2O$ can be used as a buffer of the current instantaneous loading and decrease the gas starvation phenomena because of the gas response rate that lags the loading rate to protect the fuel cell. $RuO_2 \cdot xH_2O$ can also maintain a stable PEMFC voltage when the loading current waves are within a small range.

In this study, $RuO_2 \cdot xH_2O$ was prepared by the sol–gel method and sprayed onto the Pt/C electrode surface to promote the PEMFC stack dynamic response performance. A 10-cell PEMFC stack was assembled and tested using the membrane electrode assembly (MEA) with and without $RuO_2 \cdot xH_2O$. The steady state and dynamic performance of the PEMFC stack under various operating conditions and load changes were investigated. The results showed that $RuO_2 \cdot xH_2O$ significantly increases the dynamic response performance, which is very helpful for improving the reliability of PEMFC.

2. Experimental

2.1. Preparation and characterization of $RuO_2 \cdot xH_2O$

2.1.1. Preparation of $RuO_2 \cdot xH_2O$

Sol–gel method was used to prepare $RuO_2 \cdot xH_2O$. In brief, $RuCl_3 \cdot xH_2O$ was dissolved in equal volumes of water and methanol under ultrasonication for 1 h to form organometallic species at room temperature. NaOH solution (0.1 M) was slowly added into the precursor solution until pH 7.0 was obtained. The solution was then stirred at room temperature for 30 min. The prepared precursor of the composite material was separated by centrifugation and washed 5 times with deionized water and ethanol until the Cl^- content was less than 10^{-5} mol L^{-1}. The precursor was air dried at room temperature, and then oven dried for 1 h at 150 °C for dehydration.

2.1.2. Characterization of the $RuO_2 \cdot xH_2O$ by TEM

TEM images were obtained using a JEOL TEM 2000EX microscope operated at 120 kV and 200,000 magnification to confirm the particle morphology of the $RuO_2 \cdot xH_2O$. The samples for TEM measurements were prepared by ultrasonically suspending the catalyst powder in ethanol and placing a drop of the suspension to a wholly amorphous carbon film on a Cu grid.

2.2. Preparation of MEA and assembly of a 10-cell PEMFC stack

For MEA preparation, catalyst ink was prepared by mixing the catalyst powders (40 wt.% Pt/C, E-TEK), Nafion solution, and isopropyl alcohol. Nafion 112 was used as the proton exchange membrane and Toray carbon paper was used as gas diffusion layers. The prepared catalyst ink was then sprayed onto the gas diffusion layers with Pt loading of 0.3 and 0.5 mg cm^{-2} for the anode and cathode, respectively. $RuO_2 \cdot xH_2O$ was sprayed onto the catalyst layers with a total $RuO_2 \cdot xH_2O$ loading of 0.03 mg cm^{-2}. MEAs were fabricated by placing the catalyst-coated electrodes on both sides of the pre-treated Nafion 112 membrane, and then hot pressed at 130 and 200 kg cm^{-2} for 90 s. The active area of the electrode was 270 cm^2. MEAs without $RuO_2 \cdot xH_2O$ was obtained for comparison by using the same method.

A 10-cell stack was assembled using metal composite bipolar plates and MEAs (5 MEAs with $RuO_2 \cdot xH_2O$ and 5 MEAs without $RuO_2 \cdot xH_2O$). The metal composite bipolar plates included thin metal plates as separators. The flow field parallel channel pattern was formed based on the stamped method by using expanded graphite plates. Fig. 1(a) shows the schematic diagram of the PEMFC with MEA that comprised the catalyst layer. Fig. 1(b) illustrates the

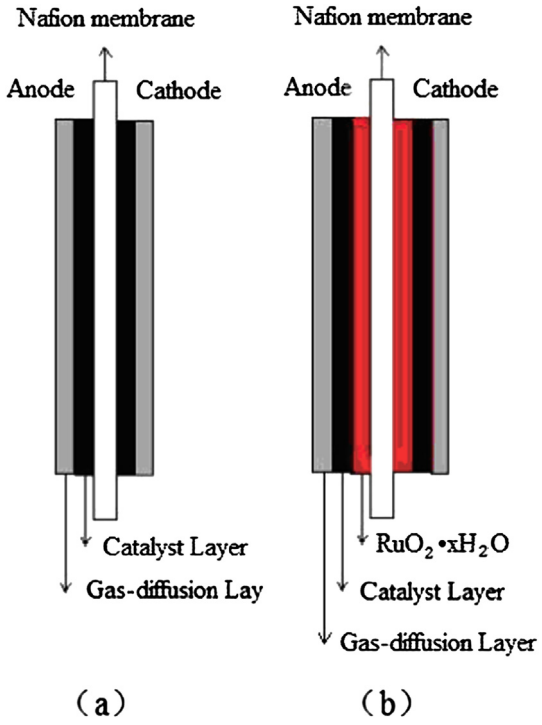

Fig. 1. Schematic diagram of PEMFC with MEAs (a) without and (b) with $RuO_2 \cdot xH_2O$.

fuel cells similar to Fig. 1(a) but with additional $RuO_2 \cdot xH_2O$ as the composite layer.

2.3. Steady state and dynamic behaviors of the PEMFC stack under various conditions

The PEMFC stack performance was tested on high-precision PEMFC testing equipment (FCATS-H36000, Hydrogenics, Canada). The experimental parameters, including fuel, oxidant, operational temperature and pressure, and stoichiometry of hydrogen and air were the same as those of the single cell. The relative humidity (RH) of the reactive gases in the PEMFC stack was accurately controlled by the dew point temperature of the reactive gases. The operational temperature and pressure of the PEMFC stack were maintained at 60 °C and ambient pressure, respectively. Each variation in the operational conditions was investigated by determining the polarization behavior and transient response of the PEMFC stack. Polarization curves were obtained by increasing the current density, allowing the fuel cell to stabilize, and measuring the PEMFC stack voltage. Transient response measurement was performed by abruptly changing the current density and measuring the time response of the voltage across the PEMFC stack. The current load was provided with the aid of an electronic load unit, which is fully computer controlled and provides the required load in a programmable method. This unit also functions as a data logger, which logs the cell response, the applied load, and the anode/cathode temperatures. Various load cycles were used in this study. The tests were run several times to ensure repeatability. Each loading condition was also repeated several times in one load cycle to assess the effect of the loading history on the cell response under a specific condition.

3. Results and discussion

3.1. Morphologies of $RuO_2 \cdot xH_2O$

The structure of $RuO_2 \cdot xH_2O$ comprises a network of rutile-like clusters with extensions in the sub-nanometer range for highly hydrated samples, along with physi- and chemi-sorbed water in its grain-boundary regions. Proton transport is facilitated by the hydrous grain-boundary regions, whereas electron transport occurs inside the $RuO_2 \cdot xH_2O$ cluster network. Amorphous ruthenium oxide, which is annealed at a critical temperature that is approximately similar to its crystalline temperature of 150 °C, shows optimum protonic and electronic conductivity. Thus, $RuO_2 \cdot xH_2O$ annealed at 150 °C [18,19] was used in the present study. The morphologies of the $RuO_2 \cdot xH_2O$ particles prepared by the sol–gel method were estimated from the TEM photographs. Typical results are shown in Fig. 2, in which the average particle size of $RuO_2 \cdot xH_2O$ is 8 nm and the particulates are uniformly distributed.

3.2. Steady-state performance of PEMFC stack

Fig. 3 illustrates the polarization curves of the PEMFC stack at the humidification temperature of 53 °C, with the air stoichiometry maintained at 2.5. These curves indicate that the performance of the MEA with $RuO_2 \cdot xH_2O$ is slightly more efficient than MEA without $RuO_2 \cdot xH_2O$. This finding is attributed to the charges that the $RuO_2 \cdot xH_2O$ provided because of its capacitance under the steady-state condition. The increased steady-state performance observed in $RuO_2 \cdot xH_2O$-incorporated electrode is caused by the increased proton conductivity in the catalyst layer. The added $RuO_2 \cdot xH_2O$ content is low; hence, the impact of $RuO_2 \cdot xH_2O$ for fuel cell performance is moderate.

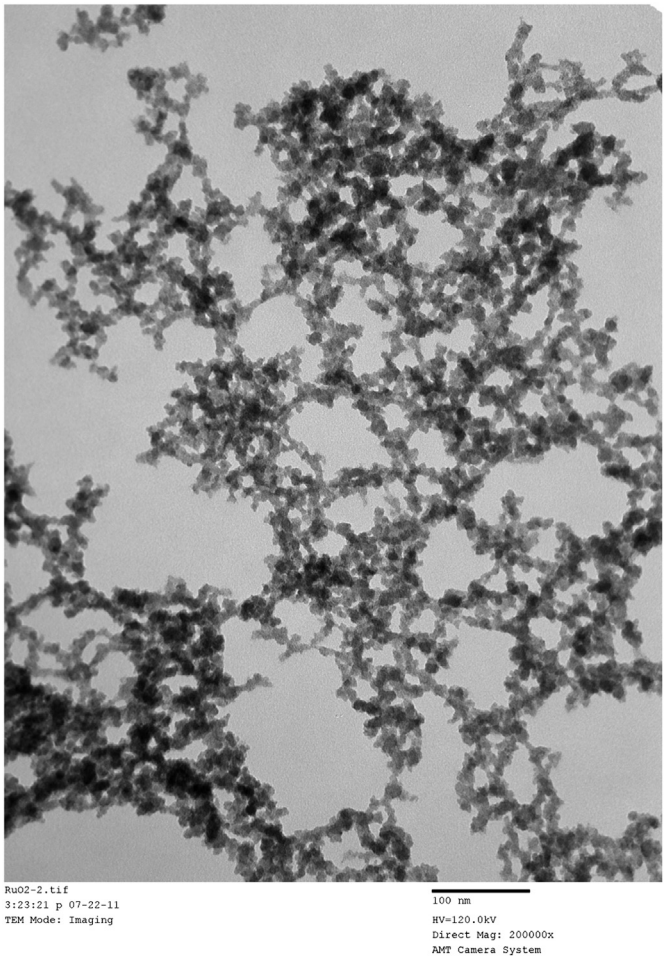

Fig. 2. TEM image of the $RuO_2 \cdot xH_2O$.

3.3. Effect of RH on PEMFC stack performance

The polarization curves at different operational RH are shown in Fig. 4. These curves indicate that the fuel cell performance was lowered at a decreasing RH from 80% to 20%. Membrane conductivity decreases at a low RH because RH of the reactant gases and the water content in the membrane is reduced. At a high current density, the transport from the anode by electro-osmotic drag

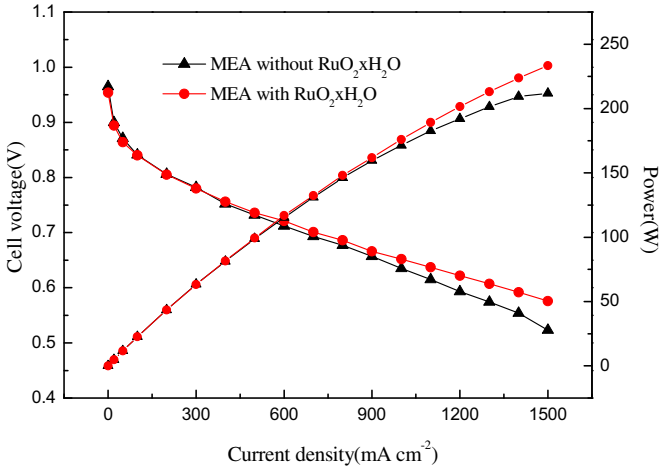

Fig. 3. PEMFC performance curves of the 10-cell stack; operating temperature = 60 °C; air stoichiometry = 2.5; relative humidity = 80%.

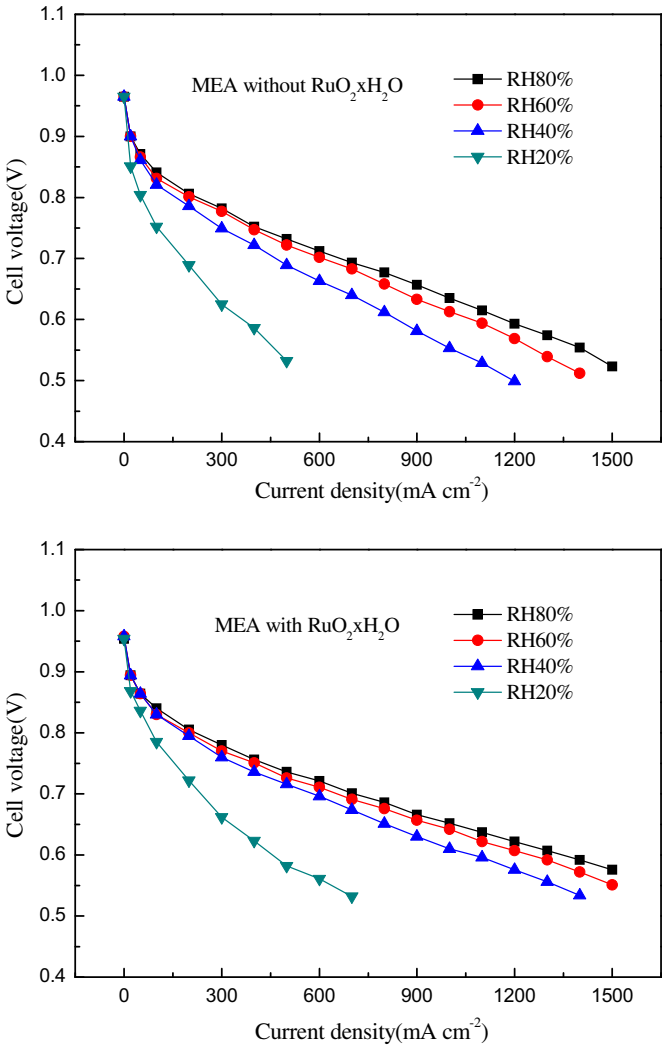

Fig. 4. PEMFC performance curves with different relative humidities; operating temperature = 60 °C; air stoichiometry = 2.5.

exceeds the transport to the anode by back diffusion from the cathode [20], thereby resulting in membrane dehydration and decreased performance. Low RH can exacerbate this effect by reducing the rate of back diffusion from the cathode.

The *I*–*V* curve of the single MEA was determined at different RH. The extent of performance decrease of the single MEA can be calculated using the following equation:

$$\text{Performance decrease (\%)} = \frac{\text{original performance(mV)} - \text{final performance(mV)}}{\text{original performance(mV)}}$$

At RH of 80%, the voltages of MEA without and with $RuO_2 \cdot xH_2O$ are 0.717 and 0.721 V, respectively, and the fuel cell performance was lowered as RH decreased. At RH of 40%, the voltage of MEA with $RuO_2 \cdot xH_2O$ at 600 mA cm^{-2} is 0.681 V (the overall decay rate was 5.5%), which was higher than that of the MEA without $RuO_2 \cdot xH_2O$ (0.658 V and 8.2%, respectively). At RH of 20%, approximately 20.1% of the cell voltage of MEA with $RuO_2 \cdot xH_2O$ was lost compared with 35.1% of MEA without $RuO_2 \cdot xH_2O$. Hence, MEA with $RuO_2 \cdot xH_2O$ has a lower decreasing rate. This rate is attributed to the charges, which were provided by $RuO_2 \cdot xH_2O$ because of its capacitance and water-retaining property under a steady-state condition at low RH [21].

3.4. Dynamic response performance of PEMFC stack under various operational conditions

3.4.1. PEMFC stack dynamic response performance under different air stoichiometry

Fig. 5 shows that the PEMFC stack performance was improved gradually as the cathode air stoichiometry increased. The air stoichiometric flow rate could influence the dynamic response performance of the PEMFC stack directly by supplying oxygen and indirectly by influencing the humidity of the membrane and water flooding. A high air flow rate increases the rate of water removal that causes the membrane to dry, thereby increasing the electrical resistance. However, the high air flow rate increases the availability of oxygen at the cathode membrane, thereby improving the performance of the fuel cell. The low air flow rate also limits the availability of oxygen because the air becomes depleted of oxygen when it reaches the end of the air flow channels. The low air flow rate can also decrease the water removal rate (liquid and vapor) and further limits the amount of oxygen that reaches the membrane. The increased gas flow rate is beneficial for the fuel cell operation if the positive effects of the increased availability of oxygen offset the negative effects of membrane dehydration [8].

Fig. 5 shows the voltage responses of MEAs with and without $RuO_2 \cdot xH_2O$ when the current density increases rapidly from 100 mA cm^{-2} to 500 mA cm^{-2} under different air stoichiometries. The fuel cell voltage undershoot behavior was observed after the current increased to 500 mA cm^{-2}. Reverse time is the time at which the output voltage of PEMFC decreases to 0 or even reaches a negative value. Recovery time is the time at which the fuel cell voltage reaches a steady-state condition. At the air stoichiometry of 1.5, the voltage undershoot (0.851 V) of the MEA without $RuO_2 \cdot xH_2O$ was evident. The instantaneous current causes the output voltage of the MEA without $RuO_2 \cdot xH_2O$ to decrease to 0 for 3 s, thereby affecting the natural life of PEMFC. The recovery time of the MEA without $RuO_2 \cdot xH_2O$ is 12 s compared with 9 s with $RuO_2 \cdot xH_2O$. The dynamic response of the cell improved when the air stoichiometry increased to 2.0 and the voltage undershoot of the MEA with $RuO_2 \cdot xH_2O$ decreased by approximately 0.618 V. MEA without $RuO_2 \cdot xH_2O$ decreased to 0 or even reached a negative value for 1 s. At air stoichiometry of 2.5, the voltage undershoots of MEAs with and without $RuO_2 \cdot xH_2O$ were 330 mV and 557 mV, respectively. Thus, lower air stoichiometry provided a poor performance and a slow transient response under the dynamic loading operation because of poor air management in the cathode of the fuel cell, which was operated at lower air stoichiometry. However, voltage responses of the MEA with $RuO_2 \cdot xH_2O$, in which the current density was increased to 500 mA cm^{-2}, became more stable at each stoichiometry. The voltage undershoot was reduced to 100–200 mV and the time for the steady state was also shortened because of the charges that the $RuO_2 \cdot xH_2O$ provided, which is attributed to the capacitance under a dynamic loading operation.

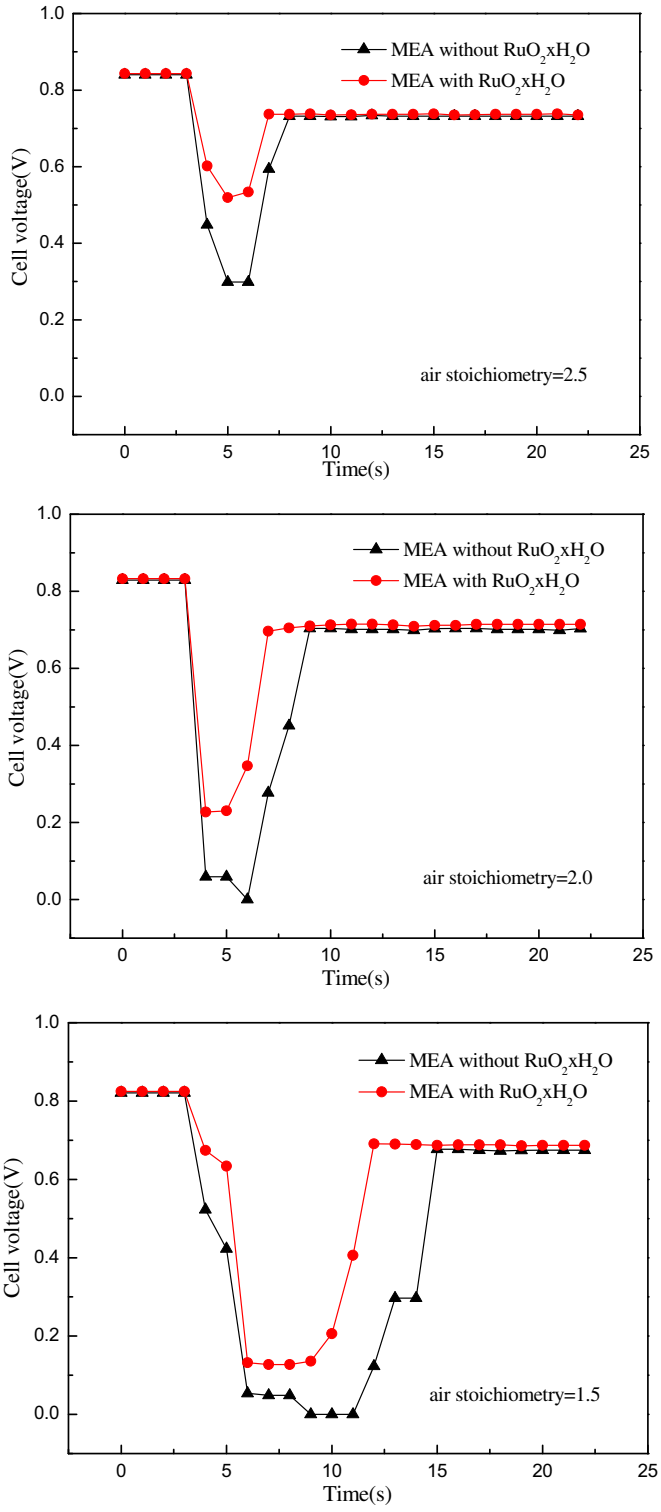

Fig. 5. Changes in voltage of MEA with and without $RuO_2 \cdot xH_2O$ with time when the dynamic loading was increased from 100 mA cm^{-2} to 500 mA cm^{-2} under different air stoichiometry; operating temperature = 60 °C; RH = 80%.

3.4.2. PEMFC stack dynamic response performance under different RH

Fig. 6 shows the dynamic response performances of the MEAs without and with $RuO_2 \cdot xH_2O$ under different RH as well as the transient voltage caused by the current steps when the fuel cell was operating at air stoichiometric flow rate of 2.5 and RH of 80%, 60%,

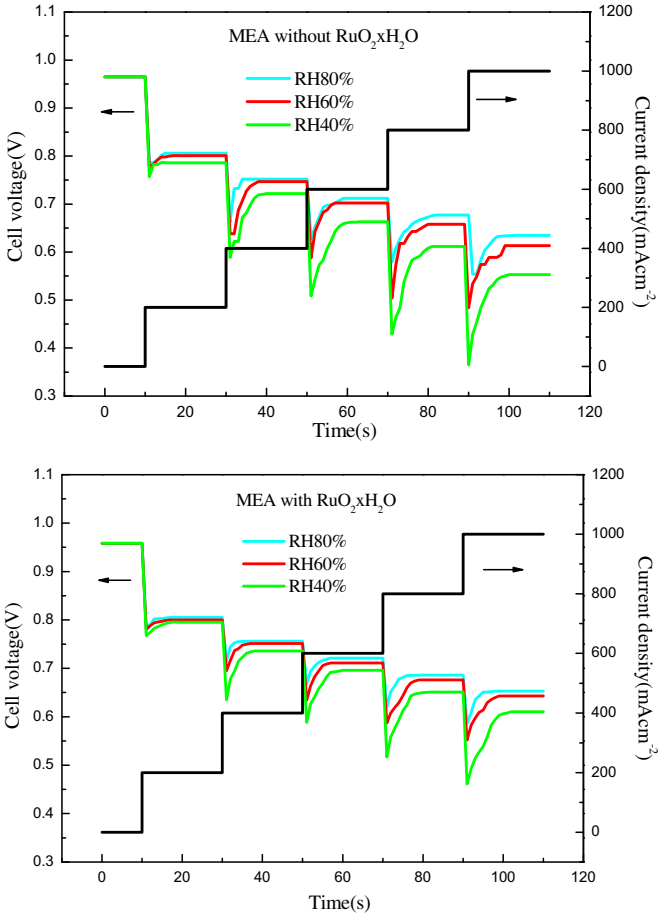

Fig. 6. Changes in voltage of MEA with and without $RuO_2 \cdot xH_2O$ with time when the dynamic loading was increased from 100 mA cm^{-2} to 500 mA cm^{-2} under different relative humidities; operating temperature = 60 °C; air stoichiometry = 2.5.

and 40%. At an operating temperature of 60 °C and RH of 40%, the MEA without $RuO_2 \cdot xH_2O$ exhibited an unstable and slower dynamic response. As the current was increased at high current densities, the voltage undershoots of the MEA without $RuO_2 \cdot xH_2O$ ranged from 150 mV to 180 mV. The MEA without $RuO_2 \cdot xH_2O$ voltage was reduced and obtained the new steady-state voltage for more than 8 s. The voltage could not be recovered for 10 s from its voltage reduction after the current increased from the current density of 800–1000 mA cm^{-2}. The MEA without $RuO_2 \cdot xH_2O$ dynamic response improved when RH was 60%. The transient response improved at RH of 80%, but the absolute voltage decreased. The MEA with $RuO_2 \cdot xH_2O$ also exhibited an unstable and slower dynamic response at RH of 40%. The voltage undershoot of the MEA with $RuO_2 \cdot xH_2O$ was 80–120 mV, and recovered in 6 s from the decrease in voltage after the current increased from the current density of 800–1000 mA cm^{-2}. The MEA with $RuO_2 \cdot xH_2O$ dynamic response was better at RH of 60%. At RH of 80%, the transient response of the fuel cell required 4 s to achieve the new stable voltage.

The fuel cell also exhibited an unstable and slower dynamic performance at lower RH for both MEAs without and with $RuO_2 \cdot xH_2O$. The voltage undershoots increased as the current increased. As RH increased to 60% and 80%, the fuel cell exhibited a fast and stable dynamic behavior for MEAs without and with $RuO_2 \cdot xH_2O$. The MEA with $RuO_2 \cdot xH_2O$ exhibited a better dynamic response at each RH because of the increase in membrane conductivity. Membrane dehydration may deteriorate the membrane. Therefore, the fuel cell dynamic performance was decreased at lower RH because of the high humidification temperatures that

directly increased the moisture content of $RuO_2 \cdot xH_2O$. The capacitance of $RuO_2 \cdot xH_2O$ was more evident. The life of a supercapacitor material is several times longer than that of an ordinary battery; hence, the supercapacitor can provide the fuel cell with sustained protection from voltage undershoots [22]. Thus, the life of the fuel cell is effectively extended.

3.4.3. PEMFC stack dynamic response performance under different loading degrees

The influence of loading degrees was investigated to understand the PEMFC stack dynamic behavior. The PEMFC stack voltage exhibited undershoots during the transient period of dynamic loading (Fig. 7). As the dynamic loading increased, the voltage undershoots also increased. The voltage undershoots of the MEAs without and with $RuO_2 \cdot xH_2O$ were 425 mV and 186 mV, respectively, after the current increased from the current density of 0–400 mA cm^{-2}. As the current increased from the current density of 0–800 mA cm^{-2}, the voltage undershoots of the MEA without $RuO_2 \cdot xH_2O$ decreased to approximately 687 mV and even reached a negative value after 2 s. The voltage required 9 s to reach a new stable voltage. The voltage undershoot of the MEA with $RuO_2 \cdot xH_2O$ only decreased to 420 mV. A layer of $RuO_2 \cdot xH_2O$ that adhered on the Pt/C electrode surface could maintain the stability of the PEMFC voltage and promote the dynamic response performance. The voltage undershoot decreases because of the lack of oxygen and the PEMFC stack voltage generally decreases to very low levels or may even reach negative values [23]. The experimental results showed that the dynamic loading affects the stability of the PEMFC stack. Therefore, the dynamic loading should be decreased at a maximum to improve the stability and lifetime of the PEMFC stack [7].

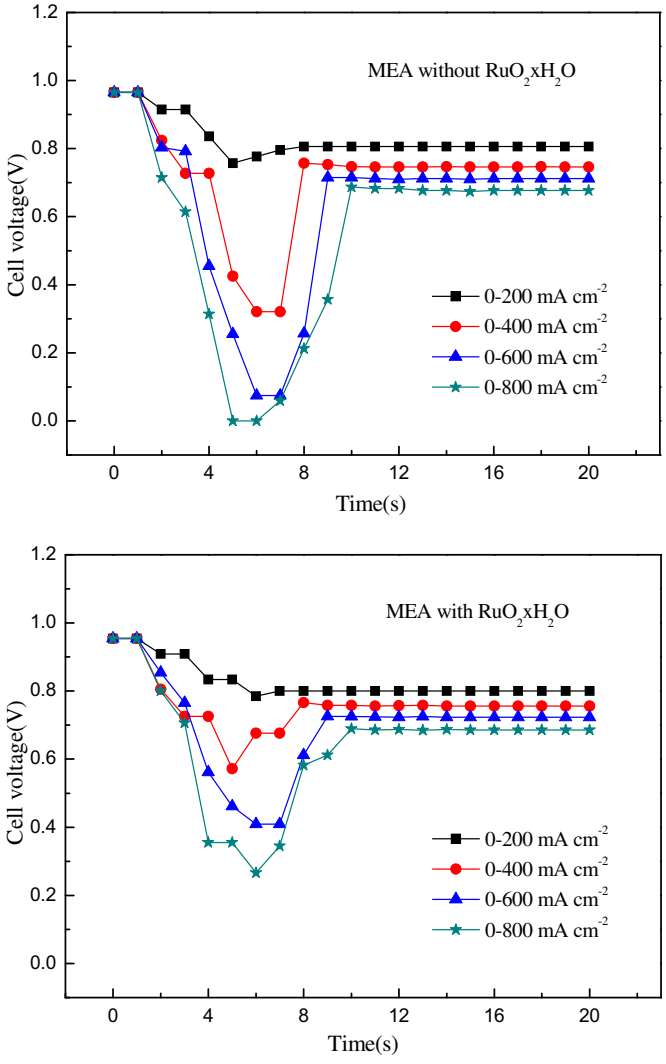

Fig. 7. Changes in voltage of MEA with and without $RuO_2 \cdot xH_2O$ with time under different dynamic loading; operating temperature = 60 °C; air stoichiometry = 2.5; relative humidity = 80%.

4. Conclusions

The dynamic response performance of the PEMFC stack is improved by spraying $RuO_2 \cdot xH_2O$ onto the catalyst layers. The TEM of the $RuO_2 \cdot xH_2O$ shows that the average particle size of $RuO_2 \cdot xH_2O$ is 8 nm and the particulates are uniformly distributed. The steady-state performance and the dynamic response performance of the PEMFC stack with and without $RuO_2 \cdot xH_2O$ are investigated under different air stoichiometry, RH, and dynamic loading. The performance of the MEA with $RuO_2 \cdot xH_2O$ is slightly better than the MEA without $RuO_2 \cdot xH_2O$. The air stoichiometry flow rate influences the PEMFC stack performance. The time required to achieve the steady state is shortened when $RuO_2 \cdot xH_2O$ is added because of the charges that the $RuO_2 \cdot xH_2O$ provide. This finding is indirectly caused by the capacitance under the dynamic loading operation. In addition, RH significantly affects the fuel cell performance. In particular, the dynamic behavior at lower RH exhibits higher voltage undershoots because of the high humidification temperatures that cause the moisture content of $RuO_2 \cdot xH_2O$ to increase directly. Thus, the capacitance of $RuO_2 \cdot xH_2O$ is more evident. A faster and more stable dynamic response can also be obtained when the MEA with $RuO_2 \cdot xH_2O$ is operated at different dynamic loading because the Faraday pseudocapacitance provided by $RuO_2 \cdot xH_2O$ functions immediately before the reactant gases are transferred to the electrode. The dynamic response performance of the MEA with $RuO_2 \cdot xH_2O$ is better than the MEA without $RuO_2 \cdot xH_2O$, indicating that the rapid charge-discharge functions of $RuO_2 \cdot xH_2O$ can effectively improve the dynamic response performance as well as the life and reliability of the fuel cell.

Acknowledgments

This research was funded by the National Basic Research Program of China (973 Program, Grant No. 2012CB215500), the National Natural Science Foundation of China (Grant No. 21176035), and Liaoning Provincial Department of Education Program (Grant No. L2010076).

References

[1] V. Mehta, J.S. Cooper, J. Power Sources 114 (2003) 32–53.
[2] P. Costamagna, S. Srinivasan, J. Power Sources 102 (2001) 242–252.
[3] J. Hana, S.M. Leea, H. Chang, J. Power Sources 112 (2002) 484–490.
[4] A. Faur Ghenciu, Curr. Opin. Solid State Mater. Sci. 6 (2002) 689–699.
[5] L.P. Jarvis, T.B. Atwater, P.J. Cygan, J. Power Sources 79 (1) (1999) 60–63.
[6] Q.Q. Gan, H.F. Xu, M.F. Zhang, Chin. J. Catal. 28 (10) (2007) 900–904.
[7] Xiqiang Yan, Ming Hou, Liyan Sun, Haibo Cheng, Youlu Hong, Dong Liang, Qiang Shen, Pingwen Ming, Baolian Yi, J. Power Sources 163 (2007) 966–970.
[8] Qiangu Yan, H. Toghiani, Heath Causey, J. Power Sources 161 (2006) 492–502.
[9] C. Wang, A.J. Appleby, J. Electrochem. Soc. 150 (2003) A493.
[10] C.C. Hu, Y.H. Huang, J. Electrochem. Soc. 146 (1999) 2465–2471.
[11] P. Zheng, J. Huang, T.R. Jow, J. Electrochem. Soc. 144 (1997) 2026–2031.
[12] S. Sarangapani, B.V. Tilak, C.P. Chen, J. Electrochem. Soc. 143 (1996) 3791–3799.
[13] G. Selvarani, A.K. Sahu, G.V.M. Kiruthika, P. Sridhar, S. Pitchumani, A.K. Shukla, J. Electrochem. Soc. 156 (1) (2009) B118–B125.
[14] F. Scheiba, M. Scholz, L. Cao, R. Schafranek, C. Roth, C. Cremers, X. Qiu, Fuel Cells 6 (2006) 439.
[15] Z. Chen, X. Qiu, B. Lu, S. Zhang, W. Zhu, L. Chen, Electrochem. Commun. 7 (2005) 593.
[16] Xi Sun, Hongfeng Xu, Huanhuan Pan, Wei Zhang, J. Mech. Eng. 45 (2) (2009) 48–50.

[17] Xiaoxin Wu, Hongfeng Xu, Lu Lu, Jie Fu, Hong Zhao, Int. J. Hydrogen Energy 35 (2010) 2127–2133.
[18] S.R. D'Souza, J. Ma, C. Wang, J. Electrochem. Soc. 153 (2006) A1795.
[19] A. Foelske, O. Barbieri, M. Hahn, R. Kotz, Electrochem. Solid-State Lett. 9 (2006) A268.
[20] T.V. Nguyen, R.E. White, J. Electrochem. Soc. 140 (8) (1993) 2178–2186.
[21] Yanbo Wu, Xiaoxin Wu, Hongfeng Xu, Lu Lu, J. Nat. Gas Chem. 20 (2011) 256–260.
[22] B. Li, J.L. Qiao, J.S. Zheng, D.J. Yang, J.X. Ma, Int. J. Hydrogen Energy 34 (2009) 5144–5151.
[23] S.D. Knights, K.M. Colbow, J. St-Pierre, D.P. Wilkinson, J. Power Sources 127 (2004) 127–133.